HHS Public Access

Author manuscript

Cancer Res. Author manuscript; available in PMC 2019 November 15.

Published in final edited form as:

Cancer Res. 2018 November 15; 78(22): 6436–6446. doi:10.1158/0008-5472.CAN-18-0659.

Astrocyte elevated gene-1 (AEG-1) regulates macrophage activation in hepatocellular carcinogenesis

Chadia L. Robertson[1], **Rachel G. Mendoza**[1], **Nidhi Jariwala**[1], **Mikhail Dozmorov**[2,3], **Nitai D. Mukhopadhyay**[2,3], **Mark A. Subler**[1], **Jolene J. Windle**[1,3], **Zhao Lai**[4], **Paul B. Fisher**[1,3,5], **Shobha Ghosh**[6], and **Devanand Sarkar**[1,3,5,7]

[1]Departments of Human and Molecular Genetics, Virginia Commonwealth University, Richmond, VA 23298, USA

[2]Departments of Biostatistics, Virginia Commonwealth University, Richmond, VA 23298, USA

[3]Departments of Massey Cancer Center, Virginia Commonwealth University, Richmond, VA 23298, USA

[4]Departments of Greehey Children's Cancer Research Institute, University of Texas Health Science Center San Antonio, San Antonio, TX 78229.

[5]Departments of VCU Institute of Molecular Medicine (VIMM), Virginia Commonwealth University, Richmond, VA 23298, USA;

[6]Departments of Internal Medicine, Virginia Commonwealth University, Richmond, VA 23298, USA;

Abstract

Chronic inflammation is a known hallmark of cancer and is central to the onset and progression of hepatocellular carcinoma (HCC). Hepatic macrophages play a critical role in the inflammatory process leading to HCC. The oncogene Astrocyte elevated gene-1 (AEG-1) regulates NF-κB activation, and germline knockout of AEG-1 in mice (AEG-1−/−) results in resistance to inflammation and experimental HCC. In this study, we developed conditional hepatocyte- and myeloid cell-specific AEG-1−/− mice (AEG-$1^{\Delta HEP}$ and AEG-$1^{\Delta MAC}$, respectively) and induced HCC by treatment with N-nitrosodiethylamine and phenobarbital. AEG-$1^{\Delta HEP}$ mice exhibited a significant reduction in disease severity compared to control littermates, while AEG-$1^{\Delta MAC}$ mice were profoundly resistant. *In vitro*, AEG-1−/− hepatocytes exhibited increased sensitivity to stress and senescence. Notably, AEG-1−/− macrophages were resistant to either M1 or M2 differentiation with significant inhibition in migration, endothelial adhesion and efferocytosis activity, indicating that AEG-1 ablation renders macrophages functionally anergic. These results unravel a central role of AEG-1 in regulating macrophage activation and indicate that AEG-1 is required in both tumor cells and tumor microenvironment to stimulate hepatocarcinogenesis.

[7]**Corresponding author:** Devanand Sarkar, 1220 East Broad St, PO Box 980035, Richmond, VA 23298, Tel: 804-827-2339, Fax: 804-628-1176, devanand.sarkar@vcuhealth.org.

Disclosure: All authors have no potential conflicts.

Keywords

AEG-1; macrophages; hepatocytes; anergy; conditional knockout mouse model

Introduction

The risk factors for HCC include viral hepatitis, alcoholism and non-alcoholic fatty liver disease all of which lead to chronic inflammation (1). Liver-resident macrophages (Kupffer cells) constitute ~20% of the total cells in the liver and play a vital role in establishing a pro-inflammatory, pro-tumorigenic environment (2). During hepatocarcinogenesis, there is also infiltration of monocyte-derived macrophages into the liver further contributing to the inflammatory process. During initial tumorigenesis, damaged hepatocytes release cytokines, such as IL-1β, which stimulate Kupffer cells to activate NF-κB resulting in the release of IL-6 that activates the oncogenic STAT3 signaling in the hepatocytes thereby promoting proliferation of transformed cells (3–10). Concomitantly, tumor-associated macrophages (resident and infiltrating) also secrete various cytokines and chemokines, including IL1-β, TNFα, IL-6, CCL2 and CXCL10, which increase HCC cell proliferation and NF-κB-mediated protection from HCC cell apoptosis, as well as angiogenic and growth factors, such as VEGF, PDGF, TGFβ and FGF, which support HCC growth (2,11). Understanding the mechanism of macrophage activation is, therefore, vital in controlling the chronic inflammatory process leading to HCC.

Our extensive studies over the last decade have firmly established that Astrocyte elevated gene-1 (AEG-1)/metadehrin (MTDH) functions as a major oncogene for HCC and is highly overexpressed in HCC patients of diverse etiologies by multiple mechanisms including genomic amplification (12–22). AEG-1 knockout mice (AEG-1−/−) exhibit complete resistance to N-nitrosodiethylamine (DEN) and phenobarbital (PB)-induced HCC (20). Furthermore, AEG-1 ablation resulted in markedly reduced inflammation in mice because AEG-1 is fundamentally required for activation of NF-κB, a key regulator of inflammatory process (20,23–26). By directly interacting with p65 subunit of NF-κB and CBP, AEG-1 functions as a bridging factor between NF-κB and basal transcriptional machinery promoting NF-κB-induced transcription (23,24). Anchored on ER membrane, AEG-1 associates with upstream ubiquitinated activators of NF-κB, such as RIP1 and TRAF2, facilitating their accumulation and subsequent NF-κB activation (25). AEG-1 is directly phosphorylated by IKKβ which is essential for IκBα degradation and NF-κB activation (26). Indeed both AEG-1−/− hepatocytes and macrophages show inherent inability to activate NF-κB upon lipopolysaccharide (LPS) treatment (20). Notably, AEG-1 itself is induced by inflammatory cytokines via NF-κB thereby establishing a positive feedback between AEG-1 and NF-κB (22,27,28).

Conversely, hepatocyte-specific AEG-1 transgenic mice (Alb/AEG-1) develop highly aggressive DEN-induced HCC compared to WT littermates indicating a key regulatory role of AEG-1 in HCC cells (18,19). AEG-1 expression in macrophages is markedly higher than that in hepatocytes (20). This observation coupled with the observations that AEG-1 is required for NF-κB activation and inflammation suggest that AEG-1 might be important for

regulating both tumor cells and tumor-associated macrophages. In the present study we interrogated the relative role of AEG-1 in these cells using tissue-specific conditional knockout mouse models. Our studies unravel a pivotal role of AEG-1 in regulating macrophage activation that profoundly affects HCC development.

Materials and Methods

Mice:

All animal studies were approved by the Institutional Animal Care and Use Committee at Virginia Commonwealth University, and were performed in accordance with the Animal Welfare Act, the PHS Policy on Humane Care and Use of Laboratory Animals, and the U.S. Government Principles for the Utilization and Care of Vertebrate Animals Used in Testing, Research, and Training. Floxed AEG-1 mice (AEG-$1^{fl/fl}$) in C57BL/6 background (20) were crossed with Alb/Cre (B6.Cg-Tg(Alb-cre)21Mgn/J) (29) and LysM/Cre (B6.129P2-*Lyz2*$^{tm1(cre)Ifo}$/J; Jackson laboratories) mice (30) to generate AEG-$1^{\Delta HEP}$ (22) and AEG-$1^{\Delta MAC}$ mice, respectively. For induction of chemical carcinogenesis, a single i.p. injection of 10 μg/gm body weight of N-nitrosodiethylamine (DEN) was given at 14 days of age to male mice and then phenobarbital (PB; 0.05%) was given daily in drinking water (20). The animals were sacrificed at 32 weeks of age. At the end of the experiment, liver, internal organs and blood were collected. Serum liver enzymes were analyzed in the VCU Molecular Diagnostic Laboratory, Department of Pathology using standard procedures. For short-term DEN treatment 2 wk old male mice were injected i.p. with DEN (10 μg/gm). Apoptosis was determined by ApoAlert DNA Fragmentation Assay kit (Takara) according to the manufacturer's protocol. For proliferation, mice were injected i.p. with BrdU (100 μg/gm; Sigma) 2 hr before sacrifice and liver sections were stained using BrdU *In-Situ* Detection Kit (BD Biosciences) according to the manufacturer's protocol.

Primary cells isolation and culture conditions:

All primary cells were used immediately after isolation in house and were mycoplasma free as detected by Mycoplasma Detection Kit (ThermoFisher). Primary mouse hepatocytes were isolated and cultured in Williams E Medium containing $NaHCO_3$, L-glutamine, insulin (1.5 mmol/L), and dexamethasone (0.1 mmol/L) as previously described (31). Kupffer cells were isolated from liver homogenates by centrifuging at 500 RPM for 10 min (32). The supernatant containing immune cells was sorted for $CD11b^+F4/80^+$ cells using FACSAria II (BD Biosciences). Bone marrow-derived macrophages (BMDM) and peritoneal macrophages were isolated according to standard protocols (33). Bone marrow cells were isolated from femurs of mice and were differentiated into macrophages using RMPI-1640 medium supplemented with 10% heat-inactivated FBS and 100U/ml recombinant mouse M-CSF for 7 days. At day 7, the media was changed to complete RPMI-1640 containing 10% heat-inactivated FBS. For isolating primary peritoneal macrophages, mice were injected i.p. with 4% thioglycollate and 4 days later macrophages were harvested in PBS via i.p. injection. Macrophages were cultured in complete media for at least 12 hours prior to using for experiments. Liver sinusoidal endothelial cells (LSEC) were purified as described using short-term selective adherence and the purity was confirmed by staining with anti-Stabilin-2 antibody (Fig. S1) (34). All primary cells were isolated from male mice of 6–12 wks of age,

were cultured at 37°C and in 5% CO_2 with 100% humidity and were used for experiments at 60–80% confluence. BMDM were treated with LPS (10 ng/ml) or IL-4 (20 U/ml) for 7 h.

Generation of Dihxy-sgAEG-1 cells:

Dihxy cells, developed from DEN-injected C57BL/6 mice, were generously provided by Dr. Michael Karin's laboratory and cultured as previously described (6). The cells were mycoplasma free as detected by Mycoplasma Detection Kit (ThermoFisher) and were not used for more than 10 passages. These cells were transfected with a plasmid expressing either control, scrambled sgRNA or AEG-1 sgRNA, Cas9, puromycin-resistance marker and mCherry (obtained from GeneCopoeia). Single clones from FACS-sorted mCherry positive cells were isolated, expanded and validated for AEG-1 knockout.

Cell proliferation assays:

Hepatocytes (1×10^4) were plated in each well of a 96 well plate for measuring proliferation by a standard MTT assay (35). For hypoxia assays, hepatocytes were cultured in 1% O_2 concentration in a hypoxic chamber (Ruskinn InVivo2 400, The Baker Company).

Efferocytosis assay:

Efferocytosis was measured using Vybrant Phagocytosis Assay Kit (ThermoFisher) according to the manufacturer's protocol.

Chemotaxis and migration assay:

Migration of macrophages toward HCC cells was performed by a modified Boyden chamber assay in which macrophages were plated on the upper chamber and HCC cells were plated on the bottom chamber and the macrophages were allowed to migrate for 24 h. Migrated cells were fixed, stained with Giemsa and counted.

LSEC adhesion assay:

LSEC ($5X10^5$) were plated in each well of an 8-chamber slide and next day macrophages ($5X10^3$) were plated on top of LSEC monolayer for 30 min following which the non-adherent cells were washed with PBS, fixed and stained using F4/80 antibody. The slides were mounted using a mounting medium containing DAPI (Vector laboratories). The images were analyzed using an Olympus microscope capturing fluorescent and bright field images.

Total RNA extraction, cDNA preparation and Real time PCR:

Total RNA was extracted from hepatocytes, macrophages or mouse tissues using the QIAGEN miRNAeasy Mini Kit (QIAGEN, Valencia, CA). cDNA preparation was done using ABI cDNA synthesis kit (Applied Biosystems, Foster City, CA). Real-time polymerase chain reaction (RT-PCR) was performed using an ABI ViiA7 fast real-time PCR system and Taqman gene expression assays according to the manufacturer's protocol (Applied Biosystems, Foster City, CA).

RNA sequencing (RNA-Seq):

Total RNA, extracted using Qiagen miRNAeasy mini kit (Qiagen, Valencia, CA) from BMDMs of 3 adult mice per group, was employed for RNA sequencing. RNA-Seq library was prepared using Illumina TruSeq RNA sample preparation kit and sequenced on Illumina HiSeq3000 platform. RNA-Seq libraries were pooled together to aim about 25–40M read passed filtered reads per sample. All sequencing reads were quality controlled using FastQC v0.11.2. Illumina adapters were trimmed using Cutadapt v1.9.dev2, replicates were merged and aligned with their reference genome (UCSC mouse genome build mm10) using subread-align v1.4.6-p4. The BAM files from alignment were processed using featureCounts v1.4.6-p4 to obtain the counts per gene in all samples. Mus_musculus.GRCm38.83.gtf gene definition file was used. The differential expression analysis was performed using edgeR v3.18.1. Genes having counts per million less than 2 in all samples were excluded. Differentially expressed genes were defined using p-value <0.01 and FDR-corrected p-value <0.1 cutoffs. All bioinformatics analyses were conducted in R/Bioconductor computing environment v3.4.0. GEO Series accession number of this dataset is GSE107691.

Western blotting analysis:

Cell lysates and tissue extracts were prepared and Western blotting was performed as described (20). The primary antibodies used were anti-AEG-1 (chicken, in-house, 1:5000), ATM (Santa Cruz, mouse monoclonal, 1:500), phospho-ATM (Cell Signaling, rabbit polyclonal, 1:1000), ATR (Cell Signaling, rabbit polyclonal, 1:1000), phospho-ATR (Cell Signaling, rabbit polyclonal, 1:1000), CHK1 (Santa Cruz, mouse monoclonal, 1:200), phospho-CHK1 (Cell Signaling, rabbit polyclonal, 1:1000), CHK2 (Santa Cruz, mouse monoclonal, 1:200), phospho-CHK2 (Cell Signaling, rabbit polyclonal, 1:1000), p53 (Cell Signaling, mouse monoclonal, 1:1000), phospho-p53 (Cell Signaling, mouse monoclonal, 1:1000), p21 (Cell Signaling, rabbit polyclonal, 1:1000) and anti-GAPDH (Santa Cruz, mouse monoclonal, 1:1000 and Cell Signaling, rabbit polyclonal, 1:1000). Densitometric analysis was performed using ImageJ software (NIH).

Immunohistochemistry (IHC) and immunofluorescence (IF) assays:

IHC was performed on formalin-fixed paraffin-embedded (FFPE) sections as described (20) using anti-AEG-1 (chicken, in-house) and anti-PCNA (Cell signaling #13110) antibodies. IF was performed on FFPE sections using anti-AEG-1 (chicken, in-house) and F4/80 (AbD Serotec #MCA497RT) antibodies. Hepatocytes were cultured in collagen-1 coated 4-chamber slides and IF was performed using antibody against γ-H2AX (Cell signaling #5438). LSEC were cultured in 8-chamber slides and IF was performed using anti-Stabilin-2 antibody (MBL International #D317–3). For IHC, images were analyzed using an Olympus microscope. For IF images were analyzed using a Zeiss confocal laser scanning microscope.

Senescence-associated β-galactosidase (SA-β-Gal) assay:

Hepatocytes were cultured for 3 days and SA-β-Gal activity was measured as described (35).

Bayesian statistical analysis:

Bayesian analysis (19) was performed to analyze the effect of hepatocyte- and macrophage-specific deletion of AEG-1 on hepatocarcinogenesis in mice. All analysis was done using the statistical computing software R v 3.3.2. The experiment measured effects of different gene mutation on liver health through a resulting tumor counts of various sizes. The notation for the responses were:

NT = number of tumors.

X1 = number of tumors of size <1 mm.

X2 = number of tumors of size 1–2 mm.

X3 = number of tumors of size 3–5 mm.

X4 = number of tumors of size 6–8 mm.

X5 = number of tumors of size above 20 mm.

In certain cases, the whole liver was reported to be tumor. In that case the response for each type of tumor size was taken to be the maximum value among all animals of that type of tumor. The covariates, or the independent variables of the experiment were type of gene mutation. The statistical model needed to accommodate a regression for counts as well as multinomial response regression. We implemented this in a Bayesian model with Poisson regression for tumor count and Multinomial regression for the observed proportion of the tumors in the 5 categories. In the notations used above, the statistical model is:

$$N_T \sim \text{Poi}(\lambda)$$

$$\log(\lambda) \sim N(\beta_0 + \beta_{HEP}(\Delta HEP) + \beta_{MAC}(\Delta MAC), \sigma_2^2)$$

$$(X_1, X_2, X_3, X_4, X_5) \mid N_T \sim \text{Multinomial}(\pi_1, \pi_2, \pi_3, \pi_4, \pi_5)$$

The structure above was implemented using a Bayesian model. All the unrestricted parameters were given flat non-informative normal prior centered at zero and variance 10^6. Posterior distribution was computed using Markov chain Montecarlo simulation with initial burn in 20,000 samples. Convergence of the model was assured using Brooks-Gelman-Rubin diagnostics. We observed multivariate PSRF = 1.05 and the PSRF for individual parameters was less than 1.1. A sample of 8,000, thinned by 3 was used to estimate the parameters of the model.

We report, instead of the estimated parameter values, the predicted values for number of tumors in each type of mice and distribution of the tumors into size categories. All estimates were obtained from the posterior distribution of the model after convergence. The summary of the MCMC outputs are shown in Tables S1-S4.

Statistical analysis:

Data were represented as the mean ± Standard Error of Mean (S.E.M) and analyzed for statistical significance using one-way analysis of variance (ANOVA) followed by Newman-Keuls test as a post hoc test.

Results

Our previous studies demonstrated profound resistance to DEN/PB-induced HCC in AEG-1−/− mice (20). Inflammation is an integral component of DEN-induced HCC and we documented that activation of NF-κB, a key regulator of inflammation, was markedly abrogated in AEG-1−/− hepatocytes and macrophages compared to AEG-1+/+ (20). In DEN-treated AEG-1+/+ livers, co-localization studies using anti-AEG-1 and F4/80 antibodies revealed increased AEG-1 in macrophages compared to hepatocytes (Fig. 1A and S2A). In DEN-treated AEG-1−/− livers, which did not show induction of HCC, F4/80 positive macrophages were sparse, compared to DEN-treated AEG-1+/+ livers (Fig. 1A and S2A). In naïve adult WT liver, higher AEG-1 staining was observed in F4/80-positive macrophages compared to hepatocytes (Fig. S2B) and AEG-1 mRNA levels in isolated Kupffer cells were ~4-times higher compared to isolated hepatocytes (Fig. S2C). These findings indicate that AEG-1 might play a regulatory role in macrophage activation during DEN-induced HCC.

To interrogate the role of hepatocyte and macrophage AEG-1 in HCC, we created hepatocyte- and myeloid cell-specific conditional AEG-1−/− mice (AEG-$1^{\Delta HEP}$ and AEG-$1^{\Delta MAC}$, respectively), by crossing AEG-$1^{fl/fl}$ mice with Alb/Cre (29) and LysM/Cre (30) mice, respectively. We have described authenticity of AEG-$1^{\Delta HEP}$ mice previously (22). AEG-$1^{\Delta HEP}$ mice were used to study the role of AEG-1 in non-alcoholic steatohepatitis but the response of AEG-$1^{\Delta HEP}$ mice to HCC development has not been studied. We now demonstrate Kupffer cell-specific AEG-1 knockout in AEG-$1^{\Delta MAC}$ mice by Taqman-Q-RT-PCR, Western blot and IHC analyses (Fig. 1B-D). AEG-1 expression was lost from F4/80-positive Kupffer cells in AEG-$1^{\Delta MAC}$ mice (Fig. 1D).

HCC was induced by DEN/PB treatment in AEG-$1^{fl/fl}$, AEG-$1^{\Delta HEP}$ and AEG-$1^{\Delta MAC}$ littermates. Control AEG-$1^{fl/fl}$ littermates, obtained by mating with either Alb/Cre or LysM/Cre mice, showed similar phenotypes and therefore the findings from all AEG-$1^{fl/fl}$ mice were clustered together. Upon treatment with DEN/PB, at 32 wks, AEG-$1^{fl/fl}$ mice developed robust multinodular HCC, AEG-$1^{\Delta HEP}$ developed HCC of significantly less magnitude than AEG-$1^{fl/fl}$ mice, while AEG-$1^{\Delta MAC}$ mice were profoundly resistant (Fig. 2A-B and Table 1). Liver weight of AEG-$1^{fl/fl}$ mice was significantly higher than that of AEG-$1^{\Delta HEP}$ and AEG-$1^{\Delta MAC}$ mice and liver weight of AEG-$1^{\Delta HEP}$ mice was significantly higher than that of AEG-$1^{\Delta MAC}$ mice as a reflection of total tumor load (Fig. 2C). To obtain additional significance, we performed Bayesian statistical analysis to check the probability of tumorigenesis using number and size of the nodules as the response variables (Fig. 2D). The probability of no tumor formation was profoundly low in AEG-$1^{fl/fl}$ mice compared to the other two groups (Fig. 2D).

H&E staining of liver sections showed HCC with loss of hepatic architecture in AEG-$1^{fl/fl}$ mice, while in AEG-$1^{\Delta HEP}$ and AEG-$1^{\Delta MAC}$ mice liver architecture was relatively well-preserved (Fig. 2E, top panel and S3). IHC staining for AEG-1 in liver sections revealed intense staining in AEG-$1^{fl/fl}$ mice, especially in the tumor, no staining in AEG-$1^{\Delta HEP}$ mice and homogenous staining in hepatocytes in AEG-$1^{\Delta MAC}$ mice (Fig. 2E, middle panel and S3). IHC staining for PCNA, a marker for cell proliferation, showed a marked increase in PCNA-positive cells in AEG-$1^{fl/fl}$ livers compared to AEG-$1^{\Delta HEP}$ and AEG-$1^{\Delta MAC}$ livers (Fig. 2E, bottom panel). Levels of serum liver enzymes, aspartate aminotransferase (AST), alanine aminotransferase (ALT) and alkaline phosphatase (AP), were significantly higher in AEG-$1^{fl/fl}$ mice *versus* AEG-$1^{\Delta HEP}$ and AEG-$1^{\Delta MAC}$ mice indicative of liver damage (Fig. 2F). The levels of mRNA for α-fetoprotein (AFP), a specific marker for HCC, were robustly higher in the livers of AEG-$1^{fl/fl}$ mice compared to the other two groups (Fig. 2G). In DEN-induced tumorigenesis, damaged hepatocytes release cytokines, such as IL-1β, which stimulate Kupffer cells to release IL-6 (3–10). Both Il1b and Il6 mRNA levels were significantly higher in AEG-$1^{fl/fl}$ livers *versus* AEG-$1^{\Delta HEP}$ and AEG-$1^{\Delta MAC}$ livers (Fig. 2G). Il1b mRNA levels were higher in AEG-$1^{\Delta MAC}$ liver compared to AEG-$1^{\Delta HEP}$ liver indicating that damaged hepatocytes in AEG-$1^{\Delta MAC}$ liver can still produce IL-1β. Il6 mRNA levels were lower in AEG-$1^{\Delta MAC}$ liver compared to AEG-$1^{\Delta HEP}$ liver indicating inhibition of macrophage activation in AEG-$1^{\Delta MAC}$ liver.

Similar to chronic liver disease, DEN treatment results in DNA damage and apoptosis in the hepatocytes (5,36). This damage triggers compensatory proliferation and repair. Upon activation of survival pathways, the damaged (and mutated) hepatocytes escape apoptosis and proliferate resulting in expansion of mutated, transformed cells. Induction of senescence in pre-malignant cells and clearing of these senescent cells by the immune system is a mechanism of HCC inhibition (37). When AEG-1−/− hepatocytes, isolated from AEG-$1^{\Delta HEP}$ mice, were deprived of growth factor, such as insulin, or subjected to stressors including H_2O_2, hypoxia and chemotherapeutic drugs, such as 5-fluorouracil (5-FU) and doxorubicin, they showed significantly increased susceptibility compared to AEG-1+/+ hepatocytes, isolated from AEG-$1^{fl/fl}$ mice (Fig. 3A-E). In *in vitro* culture mouse hepatocytes do not proliferate and enter senescence after 4 days of culture. At 3 days of culture AEG-1−/− hepatocytes, isolated from AEG-$1^{\Delta HEP}$ mice, showed marked induction of senescence, measured by senescence-associated β-galactosidase (SA-β-gal) assay and senescent-associated heterochromatic foci (SAHF) assay, compared to AEG-1+/+ hepatocytes, isolated from AEG-$1^{fl/fl}$ mice (Fig. 4A-C). *In vitro* treatment with DEN unraveled increased sensitivity of AEG-1−/− hepatocytes compared to AEG-1+/+ (Fig. 4D). DEN treatment induced DNA damage response, indicated by activation of ATM and ATR, their downstream kinases CHK1 and CHK2 leading to p53 phosphorylation and increase in p53-target p21 levels, in AEG-1+/+ hepatocytes (Fig. 4E and S4A). However, this response was markedly pronounced in AEG-1−/− hepatocytes (Fig. 4E and S4A). DNA damage response following DEN treatment was similar in hepatocytes isolated from AEG-$1^{fl/fl}$ and AEG-$1^{\Delta MAC}$ mice (Fig. S4B), indicating that it is the lack of AEG-1 in hepatocytes isolated from AEG-$1^{\Delta HEP}$ mice that confers increased susceptibility to DEN. These notion was confirmed further by *in vivo* assays, in which short term DEN treatment resulted in increased apoptosis and decreased compensatory proliferation in AEG-$1^{\Delta HEP}$ livers when

compared to AEG-1$^{fl/fl}$ and AEG-1$^{\Delta MAC}$ livers (Fig. 4F). Collectively these findings indicate that AEG-1−/− hepatocytes are more susceptible to stress and are pro-senescent so that these hepatocytes may not sustain survival and proliferation to promote the tumorigenic process thereby explaining dampened hepatocarcinogenic response in AEG-1$^{\Delta HEP}$ mice.

To understand how AEG-1 regulates macrophages so that AEG-1$^{\Delta MAC}$ mice become resistant to DEN/PB-induced HCC we analyzed differential gene expression profiles in naïve bone marrow derived macrophages (BMDM) isolated from AEG-1$^{fl/fl}$ and AEG-1$^{\Delta MAC}$ mice, by RNA-Seq. Using a false discovery rate (FDR) of <0.01 and p-value of <0.01, 1104 genes showed upregulation and 1011 genes showed downregulation in AEG-1−/− BMDM compared to AEG-1+/+ (Fig. 5A). Differentially changed genes were analyzed using Ingenuity pathway analysis software to identify the upstream regulators the activation or inhibition of which might lead to alterations in downstream genes. A z-score >2 indicates activation and a score of <−2 indicates inhibition. A highly significant (p-value <10^{-7}) and robust inhibition of upstream regulators of inflammation, immune response and cytokine signaling, such as lipopolysaccharide (LPS), interferon-γ (IFNG), tumor necrosis factor-α (TNF), interleukin (IL)-5, 2, 4, 15 and 3, toll-like receptor 4 (TLR4), lymphotoxin α (TNFSF1), myeloid differentiation primary response 88 (MYD88), inhibitor of nuclear factor kappa B kinase subunit beta (IKBKB), transforming growth factor beta 1 (TGFB1) and CpG oligonucleotides, was observed in AEG-1−/− BMDM compared to AEG-1+/+ (Fig. 5B). In addition, growth regulatory molecules, such as c-Myc and vascular endothelial growth factor (VEGFA) were also inhibited in AEG-1−/− BMDM suggesting that knocking out AEG-1 results in profound inhibition in macrophage function.

Tumor development is associated with a switch in macrophage phenotype from M1 (classically activated state), which is associated with a pro-inflammatory response, to M2 (alternatively activated), which promotes angiogenesis and tissue remodeling as well as immunosuppression (38–40). In HCC, M1 macrophages are required for the initiation of HCC while M2 macrophages are required for the sustenance of the disease. As a chronic inflammatory disease HCC livers show a flux of M1 and M2 macrophages. We treated AEG-1+/+ and AEG-1−/− BMDM, isolated from AEG-1$^{fl/fl}$ and AEG-1$^{\Delta MAC}$ mice, respectively, with lipopolysaccharide (LPS) that induces M1 differentiation. A robust increase in the mRNA levels of Il12, Il6 and iNos, markers of M1 activation, was observed in LPS-treated AEG-1+/+ BMDM but not AEG-1−/− BMDM (Fig. 5C). Similarly, IL-4 treatment to induce M2 differentiation failed to augment Il10 and Arg1, markers of M2 activation, in AEG-1−/− BMDM (Fig. 5D).

To dissect the interplay of AEG-1 in HCC cells and macrophages, we knocked out AEG-1 by CRISPR/Cas9 in mouse HCC cells Dihxy (6) (Fig. 6A). AEG-1-null Dihxy cells (Dihxy-sgAEG-1) exhibited marked decreases in proliferation compared to parental Dihxy cells and Dihxy cells expressing control, scrambled sgRNA (Dihxy-sgCon) (Fig. 6B). We treated AEG-1+/+ and AEG-1−/− BMDM, isolated from AEG-1$^{fl/fl}$ and AEG-1$^{\Delta MAC}$ mice, respectively, with conditioned medium (CM) from Dihxy-sgCon and Dihxy-sgAEG-1 cells and measured mRNA levels of M1 markers Il12, Il6, and iNos, and M2 markers Il10 and Arg1 (Fig. 6C). Upon treatment with CM from Dihxy-sgCon cells, AEG-1+/+ BMDM showed more robust induction of M2 markers Il10 and Arg1 than M1 markers, indicating

that HCC cells direct WT macrophages toward M2 differentiation. The induction of M1 and M2 markers were significantly decreased when AEG-1+/+ BMDM were treated with CM from Dihxy-sgAEG-1 cells. AEG-1−/− BMDM showed little to no induction of the M1 and M2 markers upon treatment with CM from either Dihxy-sgCon or Dihxy-sgAEG-1 cells. Collectively, these findings indicate that lack of AEG-1 renders the macrophages anergic so that they are unable to respond to any stimuli.

We next analyzed migration of AEG-1+/+ and AEG-1−/− BMDM, isolated from AEG-$1^{fl/fl}$ and AEG-$1^{\Delta MAC}$ mice, respectively, employing a Boyden chamber assay wherein BMDM were plated on the upper chamber and Dihxy-sgCon or Dihxy-sgAEG-1 cells were plated on the bottom chamber. Migration of AEG-1+/+ BMDM towards Dihxy-sgCon cells were significantly higher than that of AEG-1−/− BMDM (Fig. 6D). Additionally, migration of AEG-1+/+ BMDM towards Dihxy-sgAEG-1 cells was significantly lower than that towards Dihxy-sgCon cells, an effect further decreased in AEG-1−/− BMDM (Fig. 6D). These observations were confirmed in an *in vivo* system in which AEG-1+/+ and total AEG-1−/− mice were injected with DEN at 2 wks and transformed hepatocytes and BMDM were isolated at 12 wks. AEG-1+/+ and AEG-1−/− BMDM were treated with CM from AEG-1+/+ and AEG-1−/− hepatocytes and subjected to assays for M1 and M2 markers and migration (Fig. 6E-F). Activation of M1 and M2 markers and migration of AEG-1−/− BMDM were significantly less compared to AEG-1+/+ BMDM treated with CM from AEG-1+/+ and AEG-1−/− hepatocytes. NF-κB-regulated cytokines and chemokines, released from Dihxy-sgCon cells and AEG-1+/+ hepatocytes, stimulate migration of macrophages. AEG-1 is fundamentally required for NF-κB activation and in Dihxy-sgAEG-1 cells and AEG-1−/− hepatocytes deficiency of NF-κB-regulated cytokines and chemokines might decrease migration of AEG-1−/− macrophages. Efferocytosis is a functional activity of macrophages which was markedly inhibited in AEG-1−/− macrophages compared to AEG-1+/+ further documenting functional anergy (Fig. 6G).

Kupffer cells reside on liver sinusoidal endothelial cells (LSEC) (2). Macrophages interact with endothelial cells by means of selectin P-ligand, integrins and other cell adhesion molecules (41). Many of these genes are downstream of NF-κB and our previous study documented upregulation of these genes by AEG-1 (23). We thus hypothesize that knocking down AEG-1 might interfere with adhesion of macrophages to endothelial cells. AEG-1+/+ and AEG-1−/− Kupffer cells, isolated from AEG-$1^{fl/fl}$ and AEG-$1^{\Delta MAC}$ mice, respectively, were plated on a monolayer of LSEC, stained by F4/80 antibody and the number of F4/80-positive cells was counted (Fig. 6H-I). AEG-1−/− Kupffer cells showed significant reduction in adhesion ability compared to AEG-1+/+ Kupffer cells further establishing functional inactivation of AEG-1−/− macrophages.

Discussion

Exploiting a conditional knockout mouse system we document, for the first time, the inherent necessity for AEG-1 in macrophage activation. The functional anergy of the Kupffer cells and BMDM is similar to what is observed in normal small intestinal macrophages. The human small intestinal mucosa is characterized by resistance to inflammation, even though there is constant exposure to bacterial products, because of an

inherent anergy of intestinal macrophages which fail to respond to TLR ligands and have marked inability to activate MyD88-dependent and -independent NF-κB signaling pathway (42). In the absence of AEG-1, Kupffer cells and BMDM are unable to activate NF-κB signaling and show severe anergy so that they do not respond to any external stimuli and become functionally inactive. The basal expression of AEG-1 in human small intestine is markedly lower than that in the liver (43) suggesting that it might be the decreased level of AEG-1 that renders small intestinal macrophages anergic.

Induction of senescence in pre-malignant cells is a mechanism of HCC inhibition (37). We previously documented that Alb/AEG-1 hepatocytes show robust resistance to induction of senescence which is accompanied by dampening of induction of a DNA-damage response compared to WT hepatocytes over a period of 7 days of *in vitro* culture (18). DEN strongly activates DNA-damage signaling in hepatocytes resulting in the activation of p53 (44). We now document that *in vitro* culture-induced senescence and DEN-induced DNA-damage response are augmented in AEG-1−/− hepatocytes. AEG-1−/− hepatocytes are also more sensitive to DEN-induced cell death compared to WT. In addition, AEG-1−/− hepatocytes display a profound sensitivity to a wide variety of stressors. These findings indicate that in the absence of AEG-1, hepatocytes may not overcome apoptosis, such as those induced by DEN, so that all DEN-damaged hepatocytes die off precluding escape and survival of mutated, transformed hepatocytes. The presence of AEG-1 allows WT hepatocytes to overcome DEN-induced stress, and overexpression of AEG-1 facilitates the transformed cells ability to overcome a variety of stresses, such as hypoxia and nutrient deprivation, brought forth by the tumorigenic process. The response of AEG-$1^{\Delta HEP}$ mice to DEN is similar to that of ATM-deficient mice in which robust activation of DEN-induced ATR-Chk1-p53 renders them resistant to DEN-induced HCC (44).

Studies in mouse models have established a pivotal role of NF-κB in regulating HCC development and progression. However, the regulatory role of NF-κB is context-dependent. Mdr2−/− mice develop spontaneous cholestatic hepatitis and HCC (10,45). Overexpression of a non-degradable mutant IκBα that blocks NF-κB activation significantly inhibited HCC progression in this model (10). Hepatocyte-specific knockout of IKKβ abrogated HCC development in a transgenic mouse overexpressing lymphotoxin α and/or β (46). On the contrary, hepatocyte-specific knockout of IKKβ promoted HCC development in DEN-initiation model and hepatocyte-specific knockout of IKKγ (NEMO) resulted in spontaneous development of HCC (5,47). ROS-induced JNK and STAT3 activation has been suggested to promote HCC in IKKβ knockout model and IKKβ has been suggested to inhibit both hepatic injury and proliferation (7). However, deletion of IKKβ in macrophages significantly abrogated DEN-induced HCC (5). Additionally genetic deletion of IL-6 or inhibition of inflammatory cytokines, such as TNFα, provided a significant reduction in tumor load (8). In addition to activating NF-κB, AEG-1 activates a plethora of oncogenic signaling pathways and modulates gene expression at transcriptional, post-transcriptional and translational levels in tumor cells (48). As such, the phenotypes observed in AEG-$1^{\Delta HEP}$ mice are not corollary to hepatocyte-specific IKKβ knockout mice. On the contrary phenotypes of AEG-$1^{\Delta MAC}$ mice are similar to macrophage-specific IKKβ knockout mice, further confirming a fundamental requirement of NF-κB in macrophage activation.

The present studies indicate that targeting AEG-1 in both hepatocytes and macrophages might be an effective way in combating HCC. We recently demonstrated that hepatocyte-targeted nanoparticles delivering AEG-1 siRNA profoundly inhibited growth of orthotopic xenografts of human HCC cells in nude mice (49). In the scenario of endogenous HCC, both hepatocyte- and macrophage-targeted nanoparticles delivering AEG-1 siRNA might exert a more robust and sustained anti-HCC effect. Studies are in progress to evaluate this hypothesis.

Supplementary Material

Refer to Web version on PubMed Central for supplementary material.

Acknowledgements

DS is the Harrison Foundation Distinguished Professor in Cancer Research. PBF holds the Thelma Newmeyer Corman Chair in Cancer Research.

Financial support

The present study was supported in part by The National Institute of Diabetes and Digestive and Kidney Diseases (NIDDK) Grant 1R01DK107451–01A1 (D. Sarkar) and a Virginia Commonwealth University Massey Cancer Center pilot project grant (D. Sarkar and S. Ghosh). Services in support of this project were provided by the VCU Massey Cancer Center Transgenic/Knock-out Mouse Facility and flow cytometry core facility, supported in part with funding from NIH/NCI Cancer Center Support Grant P30 CA016059.

Abbreviations:

AEG-1	Astrocyte elevated gene-1
HCC	Hepatocellular carcinoma
DEN	N-nitrosodiethylamine
PB	phenobarbital
PCNA	Proliferating cell nuclear antigen
AFP	α-fetoprotein
LPS	Lipopolysaccharide
VEGF	Vascular endothelial growth factor
PDGF	Platelet-derived growth factor
FGF	Fibroblast growth factor
TGFβ	Transforming growth factor β
FFPE	Formalin-fixed paraffin-embedded
AST	Aspartate aminotransferase
ALT	Alanine aminotransferase

H & E	Hematoxylin and eosin
PBS	Phosphate buffered saline

Reference

1. El-Serag HB. Hepatocellular carcinoma. N Engl J Med 2011;365:1118–27 [PubMed: 21992124]
2. Krenkel O, Tacke F. Liver macrophages in tissue homeostasis and disease. Nat Rev Immunol 2017;17:306–21 [PubMed: 28317925]
3. Sakurai T, He G, Matsuzawa A, Yu GY, Maeda S, Hardiman G, et al. Hepatocyte necrosis induced by oxidative stress and IL-1 alpha release mediate carcinogen-induced compensatory proliferation and liver tumorigenesis. Cancer cell 2008;14:156–65 [PubMed: 18691550]
4. Naugler WE, Sakurai T, Kim S, Maeda S, Kim K, Elsharkawy AM, et al. Gender disparity in liver cancer due to sex differences in MyD88-dependent IL-6 production. Science 2007;317:121–4 [PubMed: 17615358]
5. Maeda S, Kamata H, Luo JL, Leffert H, Karin M. IKKbeta couples hepatocyte death to cytokine-driven compensatory proliferation that promotes chemical hepatocarcinogenesis. Cell 2005;121:977–90 [PubMed: 15989949]
6. He G, Dhar D, Nakagawa H, Font-Burgada J, Ogata H, Jiang Y, et al. Identification of liver cancer progenitors whose malignant progression depends on autocrine IL-6 signaling. Cell 2013;155:384–96 [PubMed: 24120137]
7. He G, Yu GY, Temkin V, Ogata H, Kuntzen C, Sakurai T, et al. Hepatocyte IKKbeta/NF-kappaB inhibits tumor promotion and progression by preventing oxidative stress-driven STAT3 activation. Cancer Cell 2010;17:286–97 [PubMed: 20227042]
8. Park EJ, Lee JH, Yu GY, He G, Ali SR, Holzer RG, et al. Dietary and genetic obesity promote liver inflammation and tumorigenesis by enhancing IL-6 and TNF expression. Cell 2010;140:197–208 [PubMed: 20141834]
9. Lanaya H, Natarajan A, Komposch K, Li L, Amberg N, Chen L, et al. EGFR has a tumour-promoting role in liver macrophages during hepatocellular carcinoma formation. Nat Cell Biol 2014;16:972–81, 1–7 [PubMed: 25173978]
10. Pikarsky E, Porat RM, Stein I, Abramovitch R, Amit S, Kasem S, et al. NF-kappaB functions as a tumour promoter in inflammation-associated cancer. Nature 2004;431:461–6 [PubMed: 15329734]
11. Wan S, Kuo N, Kryczek I, Zou W, Welling TH. Myeloid cells in hepatocellular carcinoma. Hepatology 2015;62:1304–12 [PubMed: 25914264]
12. Yoo BK, Emdad L, Su ZZ, Villanueva A, Chiang DY, Mukhopadhyay ND, et al. Astrocyte elevated gene-1 regulates hepatocellular carcinoma development and progression. J Clin Invest 2009;119:465–77 [PubMed: 19221438]
13. Yoo BK, Chen D, Su Z-Z, Gredler R, Yoo J, Shah K, et al. Molecular mechanism of chemoresistance by Astrocyte Elevated Gene-1 (AEG-1). Cancer Res 2010;70:3249–58 [PubMed: 20388796]
14. Yoo BK, Gredler R, Vozhilla N, Su ZZ, Chen D, Forcier T, et al. Identification of genes conferring resistance to 5-fluorouracil. Proc Natl Acad Sci U S A 2009;106:12938–43 [PubMed: 19622726]
15. Yoo BK, Santhekadur PK, Gredler R, Chen D, Emdad L, Bhutia SK, et al. Increased RNA-induced silencing complex (RISC) activity contributes to hepatocelllular carcinoma. Hepatology 2011;53:1538–48 [PubMed: 21520169]
16. Srivastava J, Robertson CL, Gredler R, Siddiq A, Rajasekaran D, Akiel MA, et al. Astrocyte Elevated Gene-1 (AEG-1) Contributes to Non-thyroidal Illness Syndrome (NTIS) Associated with Hepatocellular Carcinoma (HCC). J Biol Chem 2015;290:15549–58 [PubMed: 25944909]
17. Srivastava J, Robertson CL, Rajasekaran D, Gredler R, Siddiq A, Emdad L, et al. AEG-1 Regulates Retinoid X Receptor and Inhibits Retinoid Signaling. Cancer Res 2014;74:4364–77 [PubMed: 25125681]
18. Srivastava J, Siddiq A, Emdad L, Santhekadur P, Chen D, Gredler R, et al. Astrocyte elevated gene-1 (AEG-1) promotes hepatocarcinogenesis: novel insights from a mouse model. Hepatology 2012;56:1782–91 [PubMed: 22689379]

19. Srivastava J, Siddiq A, Gredler R, Shen XN, Rajasekaran D, Robertson CL, et al. Astrocyte elevated gene-1 and c-Myc cooperate to promote hepatocarcinogenesis in mice. Hepatology 2015;61:915–29 [PubMed: 25065684]
20. Robertson CL, Srivastava J, Siddiq A, Gredler R, Emdad L, Rajasekaran D, et al. Genetic deletion of AEG-1 prevents hepatocarcinogenesis. Cancer Res 2014;74:6184–93 [PubMed: 25193383]
21. Gong Z, Liu W, You N, Wang T, Wang X, Lu P, et al. Prognostic significance of metadherin overexpression in hepatitis B virus-related hepatocellular carcinoma. Oncol Rep 2012;27:2073–9 [PubMed: 22470125]
22. Srivastava J, Robertson CL, Ebeid K, Dozmorov M, Rajasekaran D, Mendoza R, et al. A novel role of astrocyte elevated gene-1 (AEG-1) in regulating nonalcoholic steatohepatitis (NASH). Hepatology 2017;66:466–80 [PubMed: 28437865]
23. Emdad L, Sarkar D, Su ZZ, Randolph A, Boukerche H, Valerie K, et al. Activation of the nuclear factor kappaB pathway by astrocyte elevated gene-1: implications for tumor progression and metastasis. Cancer Res 2006;66:1509–16 [PubMed: 16452207]
24. Sarkar D, Park ES, Emdad L, Lee SG, Su ZZ, Fisher PB. Molecular basis of nuclear factor-kappaB activation by astrocyte elevated gene-1. Cancer Res 2008;68:1478–84 [PubMed: 18316612]
25. Alexia C, Poalas K, Carvalho G, Zemirli N, Dwyer J, Dubois SM, et al. The endoplasmic reticulum acts as a platform for ubiquitylated components of nuclear factor kappaB signaling. Sci Signal 2013;6:ra79
26. Krishnan RK, Nolte H, Sun T, Kaur H, Sreenivasan K, Looso M, et al. Quantitative analysis of the TNF-alpha-induced phosphoproteome reveals AEG-1/MTDH/LYRIC as an IKKbeta substrate. Nat Comm 2015;6:6658
27. Vartak-Sharma N, Gelman BB, Joshi C, Borgamann K, Ghorpade A. Astrocyte elevated gene-1 is a novel modulator of HIV-1-associated neuroinflammation via regulation of nuclear factor-kappaB signaling and excitatory amino acid transporter-2 repression. J Biol Chem 2014;289:19599–612 [PubMed: 24855648]
28. Vartak-Sharma N, Ghorpade A. Astrocyte elevated gene-1 regulates astrocyte responses to neural injury: implications for reactive astrogliosis and neurodegeneration. J Neuroinflam 2012;9:195
29. Yakar S, Liu JL, Stannard B, Butler A, Accili D, Sauer B, et al. Normal growth and development in the absence of hepatic insulin-like growth factor I. Proc Natl Acad Sci U S A 1999;96:7324–9 [PubMed: 10377413]
30. Clausen BE, Burkhardt C, Reith W, Renkawitz R, Forster I. Conditional gene targeting in macrophages and granulocytes using LysMcre mice. Transgenic Res 1999;8:265–77 [PubMed: 10621974]
31. Bissell DM, Guzelian PS. Phenotypic stability of adult rat hepatocytes in primary monolayer culture. Ann NY Acad Sci 1980;349:85–98 [PubMed: 7013612]
32. Bissell DM, Guzelian PS. Degradation of endogenous hepatic heme by pathways not yielding carbon monoxide. Studies in normal rat liver and in primary hepatocyte culture. J Clin Invest 1980;65:1135–40 [PubMed: 7364941]
33. Zhang X, Goncalves R, Mosser DM. The isolation and characterization of murine macrophages. Current protocols in immunology / edited by John E Coligan [et al] 2008;Chapter 14:Unit 14 1
34. Meyer J, Lacotte S, Morel P, Gonelle-Gispert C, Buhler L. An optimized method for mouse liver sinusoidal endothelial cell isolation. Exp Cell Res 2016;349:291–301 [PubMed: 27815020]
35. Chen D, Yoo BK, Santhekadur PK, Gredler R, Bhutia SK, Das SK, et al. Insulin-like growth factor-binding protein-7 functions as a potential tumor suppressor in hepatocellular carcinoma. Clin Cancer Res 2011;17:6693–701 [PubMed: 21908579]
36. Verna L, Whysner J, Williams GM. N-nitrosodiethylamine mechanistic data and risk assessment: bioactivation, DNA-adduct formation, mutagenicity, and tumor initiation. Pharmacol Ther 1996;71:57–81 [PubMed: 8910949]
37. Kang TW, Yevsa T, Woller N, Hoenicke L, Wuestefeld T, Dauch D, et al. Senescence surveillance of pre-malignant hepatocytes limits liver cancer development. Nature 2011;479:547–51 [PubMed: 22080947]
38. Qian BZ, Pollard JW. Macrophage diversity enhances tumor progression and metastasis. Cell 2010;141:39–51 [PubMed: 20371344]

39. Mantovani A, Allavena P, Sica A. Tumour-associated macrophages as a prototypic type II polarised phagocyte population: role in tumour progression. Eur J Cancer 2004;40:1660–7 [PubMed: 15251154]
40. Lewis CE, Pollard JW. Distinct role of macrophages in different tumor microenvironments. Cancer Res 2006;66:605–12 [PubMed: 16423985]
41. Moore KJ, Tabas I. Macrophages in the pathogenesis of atherosclerosis. Cell 2011;145:341–55 [PubMed: 21529710]
42. Smythies LE, Shen R, Bimczok D, Novak L, Clements RH, Eckhoff DE, et al. Inflammation anergy in human intestinal macrophages is due to Smad-induced IkappaBalpha expression and NF-kappaB inactivation. J Biol Chem 2010;285:19593–604 [PubMed: 20388715]
43. Kang DC, Su ZZ, Sarkar D, Emdad L, Volsky DJ, Fisher PB. Cloning and characterization of HIV-1-inducible astrocyte elevated gene-1, AEG-1. Gene 2005;353:8–15 [PubMed: 15927426]
44. Teoh N, Pyakurel P, Dan YY, Swisshelm K, Hou J, Mitchell C, et al. Induction of p53 renders ATM-deficient mice refractory to hepatocarcinogenesis. Gastroenterology 2010;138:1155–65 e1–2 [PubMed: 19919837]
45. Mauad TH, van Nieuwkerk CM, Dingemans KP, Smit JJ, Schinkel AH, Notenboom RG, et al. Mice with homozygous disruption of the mdr2 P-glycoprotein gene. A novel animal model for studies of nonsuppurative inflammatory cholangitis and hepatocarcinogenesis. Am J Pathol 1994;145:1237–45 [PubMed: 7977654]
46. Haybaeck J, Zeller N, Wolf MJ, Weber A, Wagner U, Kurrer MO, et al. A lymphotoxin-driven pathway to hepatocellular carcinoma. Cancer Cell 2009;16:295–308 [PubMed: 19800575]
47. Luedde T, Beraza N, Kotsikoris V, van Loo G, Nenci A, De Vos R, et al. Deletion of NEMO/IKKgamma in liver parenchymal cells causes steatohepatitis and hepatocellular carcinoma. Cancer Cell 2007;11:119–32 [PubMed: 17292824]
48. Sarkar D, Fisher PB. AEG-1/MTDH/LYRIC: Clinical Significance. Adv Cancer Res 2013;120:39–74 [PubMed: 23889987]
49. Rajasekaran D, Srivastava J, Ebeid K, Gredler R, Akiel M, Jariwala N, et al. Combination of nanoparticle-delivered siRNA for Astrocyte elevated gene-1 (AEG-1) and all-trans retinoic acid (ATRA): an effective therapeutic strategy for hepatocellular carcinoma (HCC). Bioconjug Chem 2015;26:1651–61 [PubMed: 26079152]

Statement of Significance

Findings distinguish a novel role of macrophage-derived oncogene AEG-1 from hepatocellular AEG-1 in promoting inflammation and driving tumorigenesis.

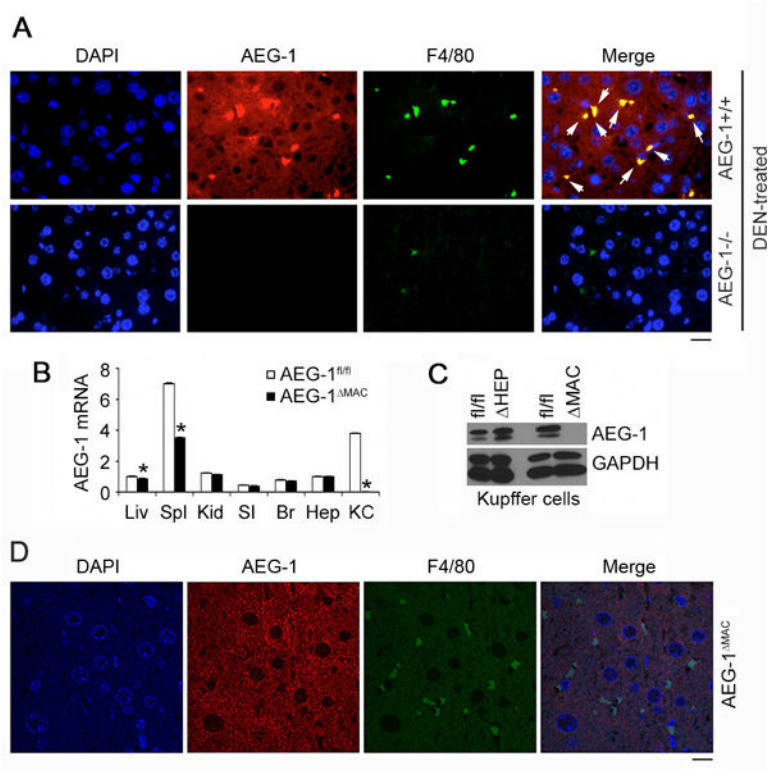

Figure 1.

Macrophages express AEG-1. A. Representative images of FFPE liver sections from DEN-treated AEG-1+/+ and AEG-1−/− mice stained with anti-AEG-1 (red) and F4/80 (green) antibodies. Yellow color in merged panels indicates localization of AEG-1 in macrophages (arrows). Magnification: 400x. Scale bar: 20 μm. B-C. Analysis of AEG-1 expression in AEG-$1^{fl/fl}$ and AEG-$1^{\Delta MAC}$ mice by Taqman Q-RT-PCR (B), Western blot analysis (C) and immunohistochemistry with anti-AEG-1 (red) and F4/80 (green) antibodies (D). For B, data were normalized by GAPDH levels. Data represent mean ± SEM; *: $p<0.01$ *vs* AEG-$1^{fl/fl}$. Liv: Liver; Spl: Spleen; Kid: Kidney; SI: Small intestine; Br: Brain; Hep: Hepatocytes; KC: Kupffer cells.

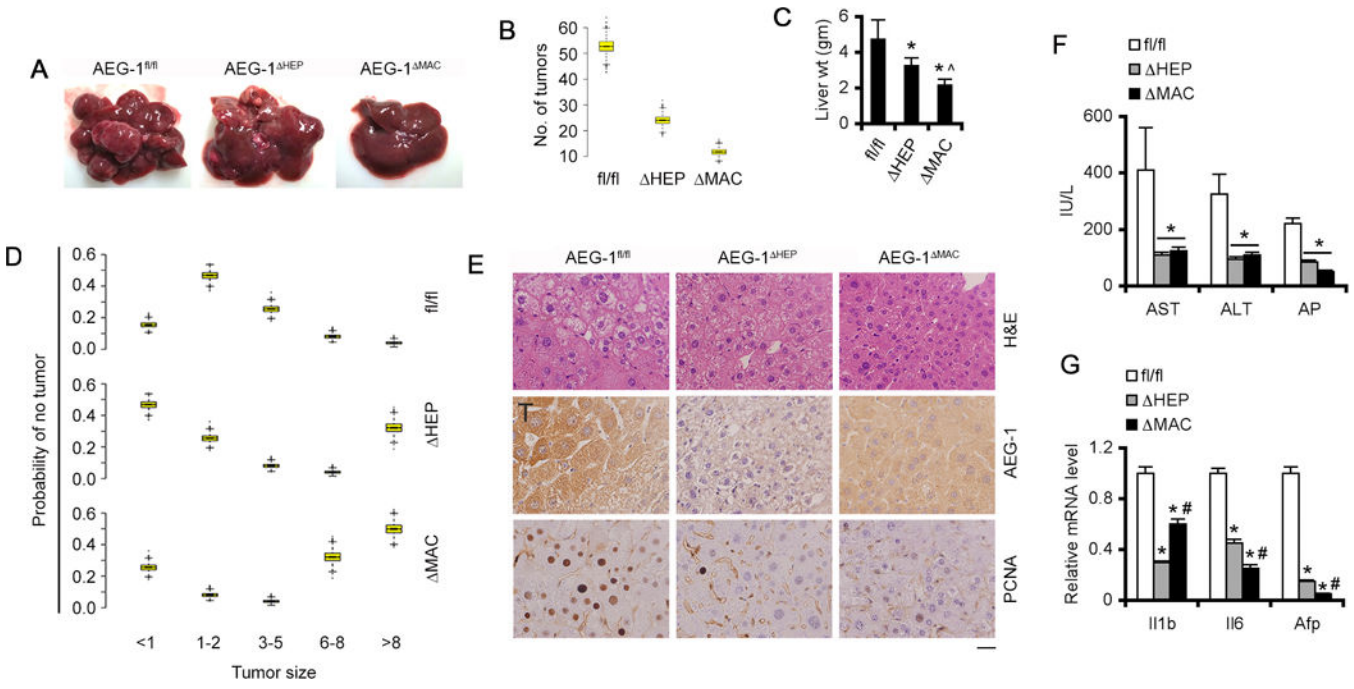

Figure 2.

AEG-1$^{\Delta HEP}$ and AEG-1$^{\Delta MAC}$ mice are resistant to experimental HCC. AEG-1$^{fl/fl}$, AEG-1$^{\Delta HEP}$ and AEG-1$^{\Delta MAC}$ mice (7 per group) received an initial DEN injection followed by PB treatment in drinking water. The mice were sacrificed at 32 weeks when all data points were analyzed. A. Representative photographs of the livers. B. Total number of tumors. C. Liver weight of the mice. Data represent mean ± SEM. *: p<0.01 *vs* fl/fl; ^: p<0.01 *vs* ΔHEP. D. Bayesian analysis demonstrating probability of no tumor. E. Top panel, H & E staining of liver sections; middle and bottom panels, AEG-1 and PCNA staining of the liver sections, respectively. Magnification: 400x. Scale bar: 20 μm. T indicates tumor. F. Serum levels of the indicated liver enzymes. AST: aspartate aminotransferase, ALT; alanine aminotransferase and AP: alkaline phosphatase. G. Relative mRNA levels of the indicated genes. GAPDH levels were used for normalization. For F-G, data represent mean ± SEM. *: p<0.01 *vs* fl/fl; #: p<0.01 *vs* ΔHEP.

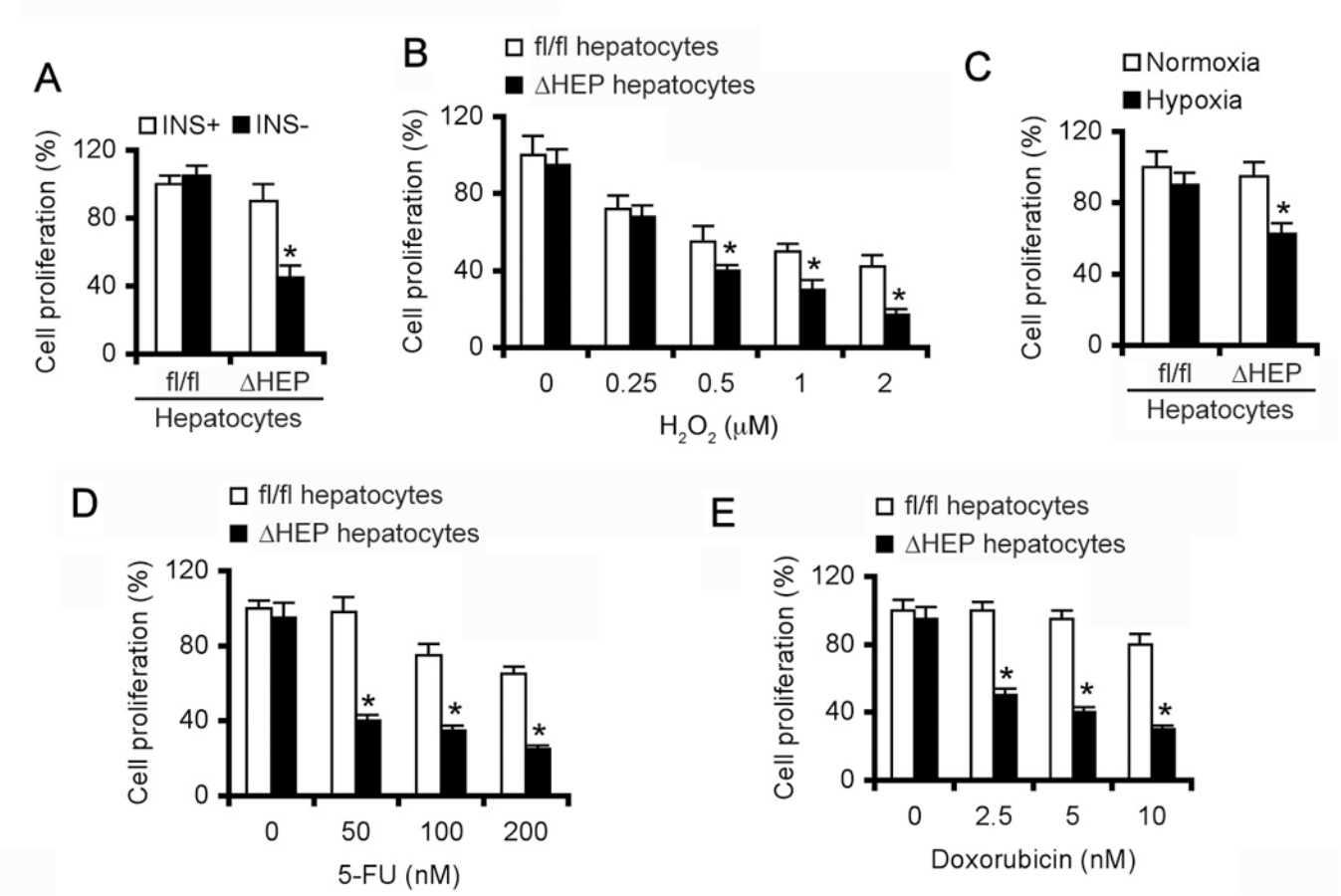

Figure 3.

AEG-1−/− hepatocytes are susceptible to stress. Proliferation of hepatocytes, isolated from AEG-$1^{fl/fl}$ and AEG-$1^{\Delta HEP}$ mice, was analyzed by MTT assay 48 h after treatment that includes insulin (INS) deprivation (A), H_2O_2 treatment at the indicated doses (B), hypoxia (C), 5-fluorouracil (5-FU) treatment at the indicated doses (D) and doxorubicin treatment at the indicated doses (E). Data represent mean ± SEM of triplicate experiments each containing 8 data points per group. *: $p<0.01$ *vs* hepatocytes isolated from AEG-$1^{fl/fl}$ mice.

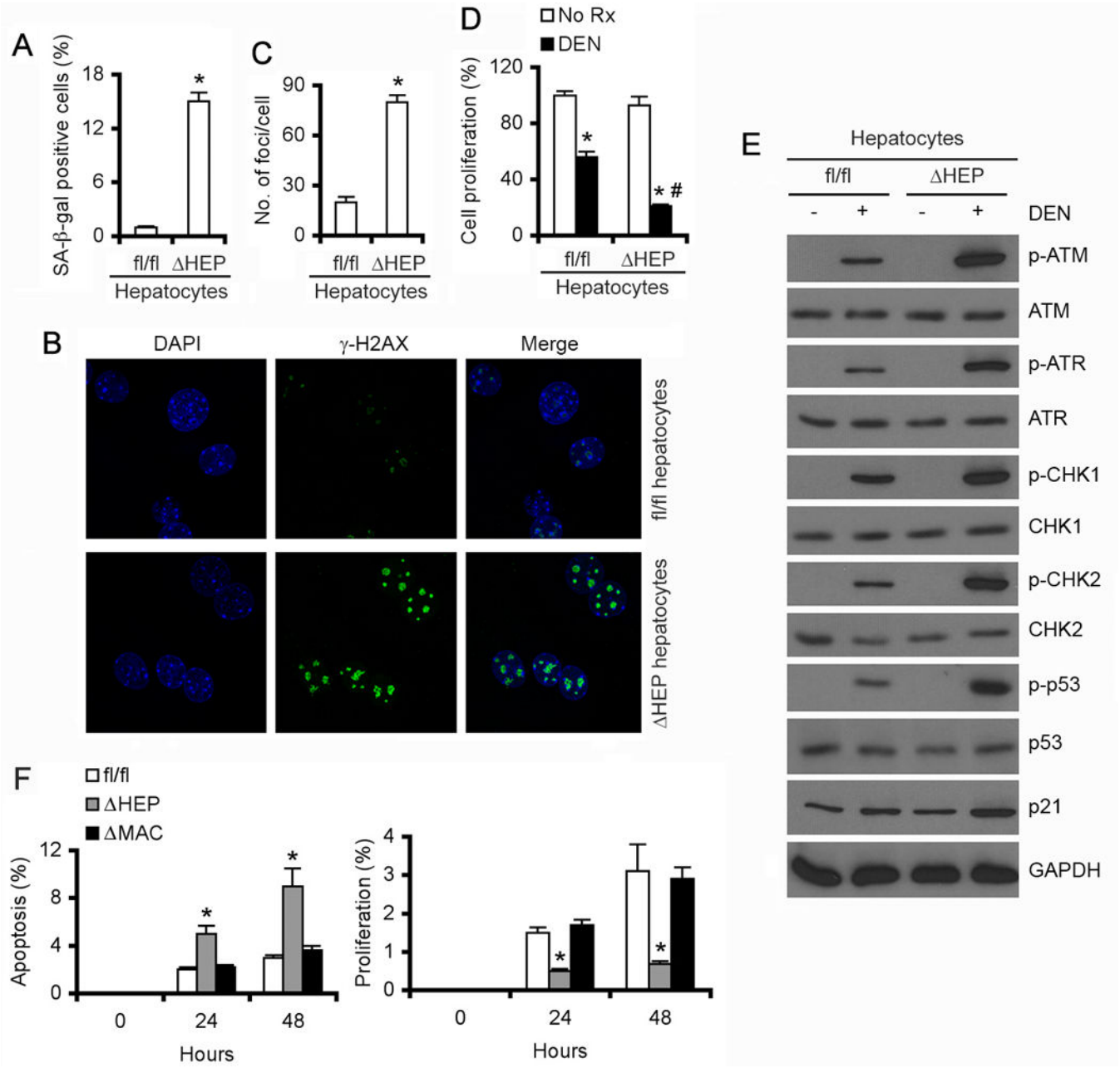

Figure 4.

AEG-1−/− hepatocytes are pro-senescent and susceptible to DEN-induced DNA damage. AEG-1+/+ and AEG-1−/− hepatocytes, isolated from AEG-$1^{fl/fl}$ and AEG-$1^{\Delta HEP}$ mice, respectively, were cultured for 3 days and senescence was determined by Senescence-associated β-galactosidase (SA-β-Gal) assay (A) and immunofluorescence (IF) staining for γ-H2AX (B-C). For B, magnification: 630x. D. Proliferation of AEG-1+/+ and AEG-1−/− hepatocytes, isolated from AEG-$1^{fl/fl}$ and AEG-$1^{\Delta HEP}$ mice, respectively, was analyzed by MTT assay 48 h after DEN (25 ng/mL) treatment. E. Western blot for the indicated proteins in AEG-1+/+ and AEG-1−/− hepatocytes, isolated from AEG-$1^{fl/fl}$ and AEG-$1^{\Delta HEP}$ mice, respectively, treated or not with DEN (25 ng/mL) for 8 h. GAPDH was used as loading

control and one representative image for GAPDH levels is shown. F. AEG-$1^{fl/fl}$, AEG-$1^{\Delta HEP}$ and AEG-$1^{\Delta MAC}$ mice were treated with DEN (10 μg/gm) and apoptosis was determined by TUNEL assay (left panel) and proliferation was determined by BrdU incorporation assay (right panel). For A and C, data represent mean ± SEM. *: $p<0.01$ *vs* hepatocytes isolated from AEG-$1^{fl/fl}$ mice. For D, data represent mean ± SEM. *: $p<0.01$ *vs* corresponding No Rx, #: $p<0.01$ *vs* hepatocytes isolated from AEG-$1^{fl/fl}$ mice. For F, data represent mean ± SEM. *: $p<0.01$ *vs* AEG-$1^{fl/fl}$ and AEG-$1^{\Delta MAC}$.

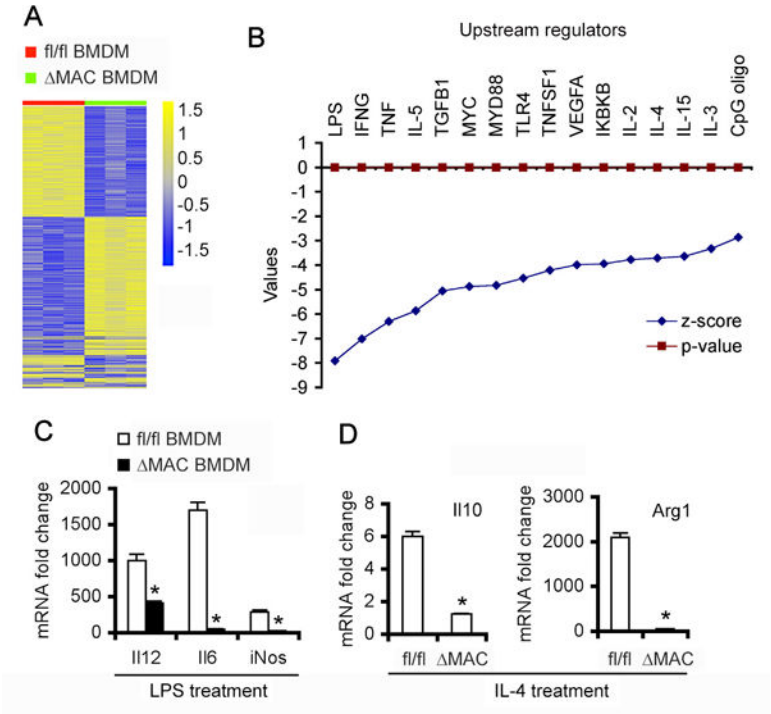

Figure 5.

AEG-1−/− macrophages resist M1 or M2 differentiation. A. Heat map of differentially expressed genes in AEG-1+/+ and AEG-1−/− bone marrow derived macrophages (BMDM), isolated from AEG-$1^{fl/fl}$ and AEG-$1^{\Delta MAC}$ mice, respectively. B. Upstream regulators inhibited in AEG-1−/− BMDM. p-value was $<10^{-7}$ thus approaching 0 in the graph. C-D. BMDM, isolated from AEG-$1^{fl/fl}$ and AEG-$1^{\Delta MAC}$ mice, were treated with 10 ng/ml LPS (C) or 20 U/ml IL-4 (D) for 7 h and the levels of the indicated mRNAs were measured by Taqman Q-RT-PCR. Data represent mRNA fold change over untreated samples and were normalized by GAPDH levels. Data represent mean ± SEM of triplicate experiments. *: $p<0.01$ *vs* BMDM isolated from AEG-$1^{fl/fl}$ mice.

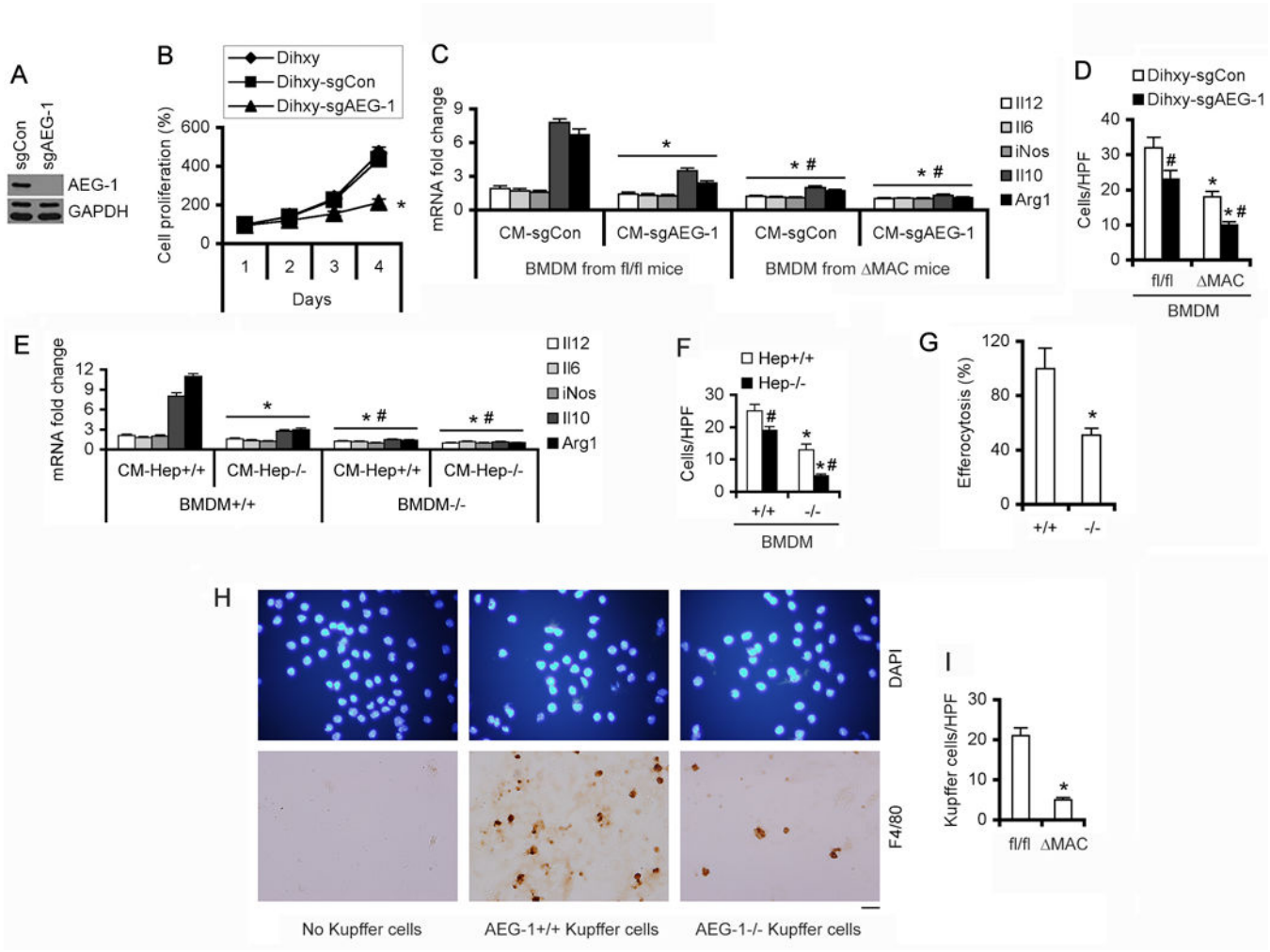

Figure 6.

AEG-1−/− macrophages show functional anergy. A. Western blot for AEG-1 in Dihxy-sgCon (sgCon) and Dihxy-sgAEG-1 (sgAEG-1) cells. B. Cell proliferation by MTT assay in the indicated clones. Data represent mean ± SEM of triplicate experiments each containing 8 data points per group. *: p<0.01 *vs* Dihxy and Dihxy-sgCon. C. AEG-1+/+ and AEG-1−/− BMDM, isolated from AEG-$1^{fl/fl}$ and AEG-$1^{\Delta MAC}$ mice, respectively, were treated with conditioned medium (CM) from Dihxy-sgCon and Dihxy-sgAEG-1 cells and the levels of the indicated mRNAs were measured by Taqman Q-RT-PCR. Data represent mRNA fold change over untreated samples and were normalized by GAPDH levels. Data represent mean ± SEM of triplicate experiments. *: p<0.01 *vs* BMDM isolated from AEG-$1^{fl/fl}$ mice treated with CM-sgCon; #: p<0.01 *vs* BMDM isolated from AEG-$1^{fl/fl}$ mice treated with CM-sgAEG-1. D. Migration of AEG-1+/+ and AEG-1−/− BMDM, isolated from AEG-$1^{fl/fl}$ and AEG-$1^{\Delta MAC}$ mice, respectively, towards Dihxy-sgCon and Dihxy-sgAEG-1 cells. Data represent mean ± SEM of triplicate experiments. *: p<0.01 *vs* corresponding AEG-1+/+; #: p<0.01 *vs* corresponding Dihxy-sgCon. E-F. AEG-1+/+ and total AEG-1−/− mice were injected with DEN (10 μg/gm) at 2 wks and transformed hepatocytes and BMDM were isolated at 12 wks. AEG-1+/+ and AEG-1−/− BMDM were treated with CM from

AEG-1+/+ and AEG-1−/− hepatocytes and the levels of the indicated mRNAs were measured by Taqman Q-RT-PCR (E). Data represent mRNA fold change over untreated samples and were normalized by GAPDH levels. Data represent mean ± SEM of triplicate experiments. *: p<0.01 *vs* BMDM+/+ treated with CM-Hep+/+; #: p<0.01 *vs* BMDM+/+ treated with CM-Hep-/−. F. Migration of AEG-1+/+ and AEG-1−/− BMDM towards AEG-1+/+ and AEG-1−/− hepatocytes. Data represent mean ± SEM of triplicate experiments. *: p<0.01 *vs* corresponding AEG-1+/+ BMDM; #: p<0.01 *vs* corresponding AEG-1+/+ hepatocytes. G. Efferocytosis of AEG-1+/+ and AEG-1−/− peritoneal macrophages. Data represent mean ± SEM of triplicate experiments. *: p<0.01. H. Representative images of adherent AEG-1+/+ and AEG-1−/− Kupffer cells, isolated from AEG-$1^{fl/fl}$ and AEG-$1^{\Delta MAC}$ mice, to liver sinusoidal endothelial cells (LSEC). Magnification: 400x. Scale bar: 20 μm. I. Quantification of adherent AEG-1+/+ and AEG-1−/− Kupffer cells to LSEC per high power field (HPF). Data represent mean ± SEM of triplicate experiments. *: p<0.01 *vs* AEG-1+/+.

Table 1.

Number and sizes of nodules in DEN/PB-treated mice at 32 weeks.

	No. of nodules (in mm)				
ID	**<1**	**1–2**	**3–5**	**6–8**	**>8**
fl/fl1	Entire liver				
fl/fl2	Entire liver				
fl/fl3	Entire liver				
fl/fl4	0	7	10	5	2
fl/fl5	0	18	1	4	2
fl/fl6	7	30	12	2	2
fl/fl7	0	25	17	1	0
ΔHEP1	*10*	*5*	*3*	*0*	*0*
ΔHEP2	*6*	*2*	*0*	*0*	*0*
ΔHEP3	*4*	*29*	*10*	*4*	*0*
ΔHEP4	*15*	*9*	*2*	*0*	*0*
ΔHEP5	*0*	*17*	*0*	*0*	*0*
ΔHEP6	*8*	*0*	*4*	*0*	*0*
ΔHEP7	*11*	*22*	*6*	*1*	*0*
ΔMAC1	5	0	0	0	0
ΔMAC2	2	0	0	0	0
ΔMAC3	8	4	0	0	0
ΔMAC4	3	11	1	0	0
ΔMAC5	10	0	4	0	0
ΔMAC6	16	5	2	0	0
ΔMAC7	5	6	0	0	0